Direct Numerical Simulation of Incipient Sediment Motion and Hydraulic Conveying

E. Papista, D. Dimitrakis, and S. G. Yiantsios*

Department of Chemical Engineering, Aristotle University of Thessaloniki, Univ. Box 453, GR 541 24, Thessaloniki, Greece

A theoretical study of the incipient sediment motion and the first stages of hydraulic transport is presented. The fluid flow and the motion of 200 heavy particles in a channel are simulated. The direct numerical simulations of fluid flow and particle motion are based on the distributed Lagrange multiplier/fictitious domain method of Glowinski et al. [*Int. J. Multiphase Flow* **1999**, *25*, 755−794). First, the particles are allowed to settle under slow flow conditions. Then, as the flow intensity is increased, which is expressed by a characteristic Reynolds number, initially intermittent and then sustained particle motion is detected at the top of the sediment. A critical Shields number is identified and compared with literature data. Further increase in flow intensity results in the increase of the number of particle layers actively participating in the motion and in their rate of transport. Moreover, the fluid flow and the moving sediment become unstable and display characteristic waves which coarsen during the course of the simulations in a way similar to the coarsening of ripples in sand beds exposed to water or air flows. A final feature of the study is the implementation of a discrete element model (DEM) to account for tangential forces and friction during the particle collisions. The collective behavior remains qualitatively the same as in a simpler model which considers only central elastic forces between the particles.

1. Introduction

Particle-laden flows are at the heart of several chemical engineering processes including fluidization, sedimentation, pneumatic, and hydraulic conveying, etc. The present work focuses on pneumatic and hydraulic conveying, which is used in a wide range of industrial areas, i.e. in the energy, food, or pharmaceutical industries, where it is frequently the only suitable method for transporting particulate material.[1−3] Related are also problems that may be encountered in some industrial processes, i.e. due to hydrate formation in oil production pipelines.[4] On a different scale and application, some pharmaceutical industries employ dry powder inhalers for drug delivery.[1,2] Thus, it is an important task in studying or designing conveying systems to identify the conditions for incipient particle motion and to select the appropriate range of fluid velocities.[1−5]

Pneumatic and hydraulic transport also occurs in a wide variety of natural phenomena, such as soil erosion and sediment transport.[6] Predicting the granular flux is important in understanding morphodynamics, i.e. how beaches, rivers, and deltas evolve, mountains erode, and landscapes form.[7,8] Among the issues central to the prediction of fluid flow and particle transport is the formation of patterns (ripples, dunes, etc.) on the erodible particle beds.[9−12] These are affected by the flow through the shear stress distribution on the bed surface and affect it through the surface roughness and the related friction experienced by the fluid.

Numerical modeling and computational fluid dynamics are today becoming important tools for the fundamental study of particle-laden flows, as well as for the design and scale up of the relevant processes. Several approaches exist,[13] which differ in the length scale of numerical resolution as compared to the length scales of the industrial equipment, the flow scales, or the size of the individual particles. For simulations at the length scale of the entire processes, it is necessary to resort to averaged equations, while as more detailed features of the flows are sought it may be feasible to employ models of interpenetrating continua, point-particle methods, or methods capable of flow resolution around the individual particles.[13−20] At one extreme of the spectrum, Direct Numerical Simulation (DNS) methods do not require any modeling of subgrid scale phenomena since they have the capability of resolving all length and time scales. Thus, DNS methods present an alternative route to experimentation for improving the understanding of fundamental issues. Several alternatives exist here as well, including boundary integral techniques[21] and Stokesian dynamics[22] for creeping flows, ALE methods with moving grids in changing geometries,[18,19] lattice-Boltzmann methods,[23,24] and immersed boundary[25] and fictitious domain methods.[20,26]

An important issue in all the above approaches is the interaction and coupling between the fluid and solid phases, which depends on the flow scales, the size of the particles, as well as their concentration.[14] At high concentrations, i.e. as encountered in fluidized beds or granular flows, the interactions between the particles may be significant or dominant and require improved degrees of realism in the modeling of particle collisions. Such improvements are introduced through the use of micromechanical models, known as discrete element models (DEM).[14,27,28] The coupling of CFD with DEM is therefore a relatively recent promising advance in the modeling of particle-laden flows.[15,29−31]

In the present study, a DNS approach is employed to simulate the initial stages of sediment motion and hydraulic transport. In this respect, the study bears some similarities to that by Choi and Joseph,[19] where the fluidization by lift and the transport of slurries was numerically studied. However, the interest there was focused on a more advanced stage of particle conveying and the parameter range was different. Another difference lies in the numerical methodology employed here. Finally, an added feature of the present work is the incorporation of a DEM model to account for particle micromechanical interactions during collisions. To the best of our knowledge, a combination of a

* To whom correspondence should be addressed. E-mail: yiantsio@auth.gr.

10.1021/ie1000828
Published on Web 06/02/2010

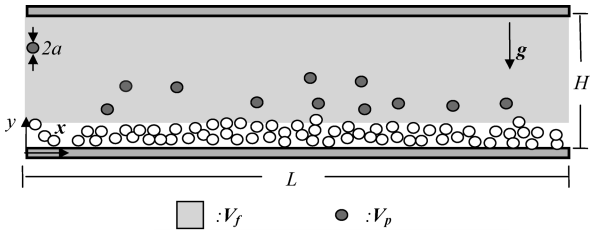

Figure 1. Definition sketch of channel flow of a fluid containing heavy particles that form a sediment. The moving fluid and the moving particles above the sediment are shaded gray.

DEM model with a DNS approach for the fluid flow has appeared in the literature only once before,[32] at the time of the writing of the present paper.

In the next section, the problem studied is rigorously defined and the governing equations for fluid flow and particle motion are stated. The main features of the numerical approach and the DEM model are also outlined. Then, in the section that follows, the main results of several simulation series are presented and discussed, whereby the flow intensity is gradually increased while the particles are transported to correspondingly increasing degrees. The relevance of the behavior obtained in the simulations to existing experimental or theoretical results from the literature is highlighted.

2. Mathematical and Numerical Formulation

2.1. Governing Equations and Dimensionless Parameters. We consider the pressure driven flow of a Newtonian and incompressible fluid in a channel between two parallel horizontal plates, separated by a distance H, as may be seen from Figure 1. Heavy particles are contained in the fluid, and thus, depending on the flow intensity, they partly settle to form a sediment near the lower plate and partly are suspended and carried by the flow.

The fluid flow is governed by the Navier−Stokes and continuity equations

$$\rho\left(\frac{\partial \mathbf{u}}{\partial t} + \mathbf{u}\cdot\nabla\mathbf{u}\right) = -\nabla P + \mu\nabla^2\mathbf{u} + \rho\mathbf{g} \tag{1}$$

$$\nabla\cdot\mathbf{u} = 0 \tag{2}$$

where ρ and μ are the fluid density and viscosity, respectively. Similarly, the motion of each particle is governed by the equations of conservation of linear and angular momentum

$$m\frac{\mathrm{d}\mathbf{U}}{\mathrm{d}t} = m\mathbf{g} + \mathbf{F}_{\mathrm{NH}} + \mathbf{F}_{\mathrm{H}} \tag{3}$$

$$I\frac{\mathrm{d}\boldsymbol{\omega}}{\mathrm{d}t} = \mathbf{T}_{\mathrm{NH}} + \mathbf{T}_{\mathrm{H}} \tag{4}$$

where m is the particle mass and I its moment of inertia. $\mathbf{F}_{\mathrm{NH}}$ and $\mathbf{T}_{\mathrm{NH}}$ are forces and torques of nonhydrodynamic origin arising during particle collisions, which are described in detail later in this section. $\mathbf{F}_{\mathrm{H}}$ and $\mathbf{T}_{\mathrm{H}}$ are respectively the force and torque exerted on each particle by the fluid, given by

$$\mathbf{F}_{\mathrm{H}} = \oint_S \boldsymbol{\sigma}\cdot\mathbf{n}\,\mathrm{d}S \tag{5}$$

$$\mathbf{T}_{\mathrm{H}} = \oint_S \mathbf{r}\times\boldsymbol{\sigma}\cdot\mathbf{n}\,\mathrm{d}S \tag{6}$$

Here S is the particle surface, $\mathbf{n}$ the unit normal vector pointing to the fluid, $\mathbf{r}$ is the vector joining the particle center of mass to its surface, and $\boldsymbol{\sigma}$ is the fluid stress tensor

$$\boldsymbol{\sigma} = -P\mathbf{I} + \mu[\nabla\mathbf{u} + (\nabla\mathbf{u})^{\mathrm{T}}] \tag{7}$$

Continuity of velocities on the particle surface dictates that

$$\mathbf{u} = \mathbf{U} + \boldsymbol{\omega}\times\boldsymbol{r} \tag{8}$$

where $\boldsymbol{\omega}$ is the particle rotation rate.

A two-dimensional (2D) model is considered with circular disks of radius a and density ρ_{P} representing the particles, and the flow is driven by a constant pressure gradient, $\Delta P/\Delta L$. In the simulations the following fixed values have been chosen: $a/H = 0.04$ and $\rho_{\mathrm{P}}/\rho = 2$. The channel height, H, is chosen as the characteristic length, and the maximum velocity of a particle-free fluid under laminar flow conditions as the characteristic velocity, which is the following:

$$U_0 = (\Delta P/\Delta L)H^2/8\mu \tag{9}$$

Then, the time unit is H/U_0, and the pressure unit is $1/2\rho U_0{}^2$. Introducing this scaling, the only dimensionless parameter appearing in the Navier−Stokes equations is the Reynolds number

$$Re = \rho U_0 H/\mu \tag{10}$$

while the dimensionless constant pressure gradient is given by

$$\Delta\hat{P}/\Delta\hat{L} = 8/Re \tag{11}$$

Due to the difference in particle and fluid density, an additional parameter appears in the particle equations of motion, which is the Froude number

$$Fr = \frac{\Delta\rho g H}{\rho U_0{}^2} = \frac{\rho\Delta\rho g H^3/\mu^2}{Re^2} = \frac{Ar}{Re^2} \tag{12}$$

Here, Ar is the Archimedes number. In the present simulations, Ar is taken as constant and equal to 10^6.

In summary, apart from the particle concentration, seven physical parameters describe the present problem (H, ρ, μ, ρ_{P}, a, g, $\Delta P/\Delta L$), which combine into four dimensionless parameters (a/H, ρ_{P}/ρ, Fr, Re or a/H, ρ_{P}/ρ, $\mathrm{A}r$, Re). In the present study, fixed values are given to the first three, as mentioned above, and the focus is on the effect of the flow Reynolds number.

As is usual practice in simulations of similar kind in the literature, a finite channel length, L, is considered and periodic conditions are employed.[19,23,24] In the present simulations L/H is taken to be equal to 4. The number of particles considered within each periodic channel segment is 200.

2.2. Numerical Method. The numerical approach for the discretization and solution of the governing equations is based on the Galerkin finite element method. More specifically, a methodology is applied known as distributed Lagrange multiplier/fictitious domain method (DLM/FDM), which was proposed for the direct numerical simulation of particle-laden multiphase flows or flows containing moving solids.[20,33] A variational formulation of the governing equations was developed, which is particularly suitable for finite element implementations. The particularly attractive characteristic of the methodology is that a fixed numerical grid is employed, which does not need to coincide with the surfaces of the immersed solid bodies. In this way, the extremely difficult and computationally intensive task of discretizing an ever-changing geometry is overcome. Numerical simulations for the sedimentation of as many as 5000 particles in Newtonian and non-Newtonian fluids, the flow of neutrally buoyant particles in channels and pipes, and the

fluidization of more than 1000 particles have appeared in the literature.[33−35]

Very briefly, the basic idea is to fill the space occupied by the particles by a hypothetical fluid similar to the surrounding fluid. Thus, the flow equations are solved in a much simpler geometry. Point forces (the Lagrange multipliers) are distributed in the fictitious domain of the hypothetical fluid and force it to move as a solid body, in the same way as the real immersed particles translate and rotate. In the final stage, the principles of linear and angular momentum conservation are satisfied by applying equal and opposite forces (and the corresponding torques) to the solid particles, which translate and rotate in response to real forces, such as gravity, and the Lagrange multipliers. For more details, the reader is referred to the cited references.

In the present implementation, the operator splitting scheme proposed by Glowinski et al.[20] for the integration of the equations is followed with minor modifications. The same triangulation is employed for both velocity and pressure, which are represented by quadratic and linear polynomials (a P_2-P_1 scheme) in each spatial direction, respectively. In the first substep of the splitting scheme, a second order Adams−Bashforth procedure is applied to handle the advection terms. In the second substep the pressure field is calculated and incompressibility is enforced. Here, the viscous terms are also included and the conjugate gradient algorithm is employed for the iterations. In the final substep the Lagrange multipliers are calculated and the velocities of fluid and particles are updated. An iterative scheme based on the conjugate gradient algorithm is applied here as well.

For the flow domain of the present problem, a simple triangulation was employed with velocity nodes spaced at 1/100 of the channel height, resulting in 40 000 unknowns for each velocity component. The distance between pressure nodes was 1/50, and the corresponding unknowns were 10 000. A constant dimensionless time step equal to 0.001 was used in all the simulations. Finally, 40 Lagrange multipliers were evenly distributed on concentric circles within the domain of each particle. The concentric circles and the collocation points on each circle are placed at distances approximately equal to the flow grid. A number of tests on the adequacy of numerical resolution was performed by employing a finer grid with 800 × 200 nodes for the velocity and 144 Lagrange multipliers within each particle. In addition, some tests where performed with the periodicity interval doubled and a grid of 800 × 100 nodes.

2.3. Particle Interactions-mDEM. Particle overlapping is usually a problem in simulations of particle laden flows, even when lubrication forces are explicitly taken into account, i.e. in Stokesian dynamics.[22] In order to prevent this unphysical behavior, it is usual practice in the simulations to employ nonhydrodynamic central forces, which are activated when the particles are in close approach. In real systems, such forces may be due to contact between roughness elements and asperities or due to electrostatic and other interactions of colloidal nature. Pan et al.[32] discuss the fundamental and practical aspects of this problem and suggest a procedure where a spherical shell with size of the order of the numerical grid surrounds each particle. Then a distance-dependent force repels the particles when their shells overlap. In most of the present simulations, we employed the same procedure with central forces between particles in near contact, as well as between particles and the bounding surfaces of the channel.

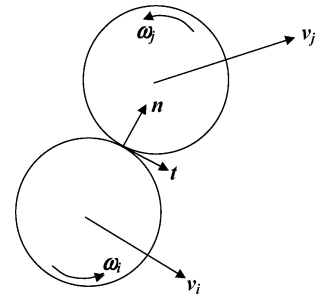

Figure 2. Definition sketch for a collision between two particles.

However, in real systems, the interactions during particle collisions are more complex. Kinetic energy is dissipated, and tangential forces, as well as couples on the particles, arise. Moreover, these interactions may play a significant or dominant role in the behavior of the particle-laden multiphase system. Tsuji[14] discusses several applications of particle-laden flows and discriminates between three different classes of behavior, namely (a) the *collision-free* flows, (b) the *collision-dominated* flows, and (c) the *contact-dominated* flows. According to this classification it is suggested there that pneumatic and hydraulic transport of particles may fall in the second category.

Therefore, in order to have an improved degree of realism in the particle interactions and explore possible effects of such interactions a DEM was employed in some simulations.[27,28] DEMs for particle interactions have been used before in the literature in conjunction with computational fluid dynamics (CFD) simulations. However, the existing simulations usually employ a volume-averaged approach for the flow description.[29−31] As stated already, a combination of a DEM model with a DNS approach for the fluid flow has only appeared once in the literature recently.[32]

In the particular model, with reference to Figure 2, the normal and tangential relative velocities at the contact point are

$$v_n = (v_j - v_i) \cdot \mathbf{n} \tag{13}$$

$$v_t = [(v_j - v_i) + \boldsymbol{\omega}_j \times \mathbf{r}_j - \boldsymbol{\omega}_i \times \mathbf{r}_i] \cdot \mathbf{t} \tag{14}$$

Here, $\mathbf{n}$ and $\mathbf{t}$ are the unit vectors parallel and normal to the line of particle centers, respectively, and $\mathbf{r}_i$ and $\mathbf{r}_j$ are the vectors joining the particle centers with the contact point.

The central or normal nonhydrodynamic force on particle j has the form

$$F_{\mathrm{NH},n} = -c_1 \cdot \Delta n - c_2 v_n \tag{15}$$

where Δn is the deformation along the line of particle centers at the contact point and c_1, c_2 are constants of the linear model. The first term represents elastic interactions and the second viscous, irreversible interactions.

During a collision, the tangential displacement, s, of the contact point is given by

$$\frac{\mathrm{d}s}{\mathrm{d}t} = v_t \tag{16}$$

and in a similar fashion the tangential force on particle j is

$$F_{\mathrm{NH},t} = -c_3 s - c_4 v_t \tag{17}$$

Finally, rolling friction is also accounted for in the present model, following the work of Iwashita et al.,[27] who introduced the term mDEM or micro-discrete element model. If θ is the angle of relative particle rotation at the contact point, then

$$\frac{\mathrm{d}\theta}{\mathrm{d}t} = \left(\boldsymbol{\omega}_j \times \frac{\mathbf{r}_j}{|\mathbf{r}_j|} - \boldsymbol{\omega}_i \times \frac{\mathbf{r}_i}{|\mathbf{r}_i|}\right) \cdot \mathbf{t} \tag{18}$$

and the nonhydrodynamic torque on particle j is modeled by

$$\mathbf{T}_{\mathrm{NH}} = aF_t - c_5\theta - c_6\frac{\mathrm{d}\theta}{\mathrm{d}t} \tag{19}$$

Finally, as is standard practice in DEM models, if the tangential force and the torque exceed a certain threshold, the respective expressions are replaced by Coulomb's friction law, i.e.

$$F_{\mathrm{NH},t} = -\mu F_{\mathrm{NH},n} \tag{20}$$

and

$$T_{\mathrm{NH}} = -\mu_t F_{\mathrm{NH},n} \tag{21}$$

It must be noted that the deformations mentioned above are assumed infinitesimal compared to the particle size and flow grid. In the numerical implementation, they are defined in terms of the position of the particle centers and their rotation rates. Hence, from the perspective of the simulation of the fluid and particle motion, the particles remain perfectly spherical.

2.4. Shear Stress on the Sediment Surface and Shields Number. The Shields number is a dimensionless parameter which compares the relative weight of the particles to the force exerted on them by the fluid flow. It is used as a criterion for correlating the condition for incipient particle motion in erodible noncohesive sediments[3,4,36] and is defined by the relation

$$\theta = \frac{\tau_{\mathrm{s}}}{2\Delta\rho g a} \tag{22}$$

where τ_{s} is the shear stress exerted by the fluid on the top of the sediment.

In order to obtain a nominal value of the shear stress at the sediment surface the following procedure is applied, which is based on the application of integral momentum balances. A control volume is selected, which is part of the periodic computational cell and includes the moving fluid and the moving particles. Thus, as shown in Figure 1, the control volume (shaded in gray) is bounded by the two periodic vertical sides normal to the mean flow direction, the upper fixed plate and the surface of the motionless sediment. This volume is the sum of the fluid volume, V_{f}, and the volume of n moving particles, nV_{p}.

Integrating the fluid momentum equation over the fluid volume V_{f} and applying Green's theorem, we obtain

$$\int_{V_{\mathrm{f}}} \rho \frac{\partial \mathbf{u}}{\partial t}\,\mathrm{d}V = -\Delta P S \mathbf{e}_x + \mathbf{F}_{\mathrm{uw}} + \mathbf{F}_{\mathrm{s}} - \sum_n \mathbf{F}_{\mathrm{H}} + \int_{V_{\mathrm{f}}} \rho \mathbf{g}\,\mathrm{d}V \tag{23}$$

where S is the cross-sectional area of the control volume and $\mathbf{F}_{\mathrm{uw}}$ and $\mathbf{F}_{\mathrm{s}}$ are the forces exerted on the fluid by the upper wall and the sediment, respectively.

Employing the particle momentum equations, we eliminate the hydrodynamic forces on the n moving particles to obtain

$$\int_{V_{\mathrm{f}}} \rho \frac{\partial \mathbf{u}}{\partial t}\,\mathrm{d}V + \left(\sum_n \rho_{\mathrm{P}} \frac{\mathrm{d}\mathbf{U}}{\mathrm{d}t}\right)V_{\mathrm{p}} = -\Delta P S \mathbf{e}_x + \mathbf{F}_{\mathrm{uw}} + \mathbf{F}_{\mathrm{s}} + \int_{V_{\mathrm{f}}} \rho \mathbf{g}\,\mathrm{d}V + \sum_n \rho_{\mathrm{P}} \mathbf{g} V_{\mathrm{p}} \tag{24}$$

Since according to the DLM/FDM method a fluid velocity is calculated within the particle domain, the momentum terms above may be written in the form

$$\int_{V_{\mathrm{f}}} \rho \frac{\partial \mathbf{u}}{\partial t}\,\mathrm{d}V + \left(\sum_n \rho_{\mathrm{P}} \frac{\mathrm{d}\mathbf{U}}{\mathrm{d}t}\right)V_{\mathrm{p}} = \rho \frac{\mathrm{d}}{\mathrm{d}t}\int_{V_{\mathrm{T}}} \mathbf{u}\,\mathrm{d}V + \left(\sum_n \Delta\rho \frac{\mathrm{d}\mathbf{U}}{\mathrm{d}t}\right)V_{\mathrm{p}} \tag{25}$$

The first term represents the rate of change of fluid momentum in the real and hypothetical domain. The second term is the rate of change of excess particle momentum due to their higher density.

Finally, if the mean flow direction is considered, the gravity terms in eq 24 do not play a role and the forces are expressed in terms of shear stresses we obtain in dimensionless form

$$\frac{\mathrm{d}}{\mathrm{d}t}\int_{V_{\mathrm{T}}} u\,\mathrm{d}V + \left(\sum_n \frac{\Delta\rho}{\rho}\frac{\mathrm{d}U}{\mathrm{d}t}\right)V_{\mathrm{p}} = -(1-\hat{h})\Delta\hat{P} + \frac{1}{Re}(\hat{\tau}_{\mathrm{uw}}\hat{L} + \hat{\tau}_{\mathrm{s}}\hat{L}) \tag{26}$$

where $\hat{h}$ is the sediment height. The latter is obtained from the average velocity field as the height below which the velocity in the flow direction is nominally zero. The above equation may be solved for the nominal shear stress at the sediment surface, since all the other terms may be obtained directly from the simulation. Using the dimensionless parameters that have already been defined and given fixed values in the present simulations, the Shields number may then be written as

$$\theta = \frac{\hat{\tau}_{\mathrm{s}}(\mu U_0/H)}{2\Delta\rho g a} = \hat{\tau}_s \frac{\rho U_0 H}{\mu}\frac{\mu^2}{\rho\Delta\rho g H^3}\frac{H}{2a} = \hat{\tau}_{\mathrm{s}}\frac{Re}{Ar}\frac{1}{2\hat{a}} = \hat{\tau}_{\mathrm{s}}\frac{Re}{8\times 10^4} \tag{27}$$

3. Results and Discussion

Results from six series of simulations covering the range of Reynolds numbers between 3500 and 8000 are presented in this section. Initially the particles were randomly placed in the channel and allowed to settle at a sufficiently low Reynolds number, so that a motionless sediment was formed. Then, the Reynolds number was progressively increased until some particles started to saltate. Each simulation series proceeded until a statistically steady state was reached. The final state was then used as an initial condition for a new series at an increased Reynolds number. Each time unit corresponds approximately to 1 h of computer time on a personal computer, and this may be used to give an idea of the time invested in obtaining the results that follow. The simulations in the following three subsections employ a simple central elastic force model for the nonhydrodynamic interactions between particles during collisions. Then, in the last subsection, results with the more complete DEM are discussed.

3.1. Incipient Particle Motion and Critical Shields Number. In Figure 3, the mean particle velocity in the main flow direction is presented as a function of time for Reynolds numbers equal to 3000 and 3500. It is observed that for $Re = 3500$ sustained particle motion takes place. Therefore, these conditions can be identified as the conditions for incipient motion in the present simulations.

The nominal values of the shear stress on the sediment surface were calculated on the basis of eq 26. These, together with the corresponding Shields numbers, are shown in Table 1.

The onset, therefore, of particle motion in the present simulations corresponds to a critical Shields number of 0.14. On the basis of data from the relevant literature, it may be observed that the critical Shields numbers is lower than unity and rather close to 0.1, although a universal constant value does

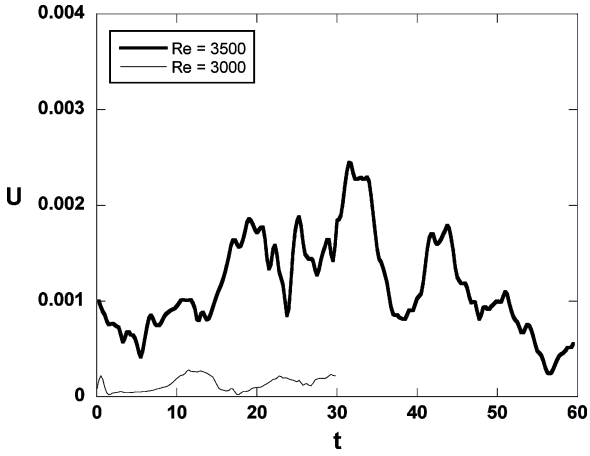

Figure 3. Average particle velocity as a function of time for the Reynolds numbers indicated.

Table 1. Shear Stress on Sediment and Shields Number As Functions of the Reynolds Number in the Simulations

Re	3500	4000	5000	6000	7000	8000
$\hat{\tau}_s$	3.3	3.5	3.9	4.4	5.1	5.6
θ	0.14	0.18	0.25	0.33	0.44	0.56

not exist. Loiseleux et al.[36] and Kuru et al.[3] present collections of bibliographical data, as well as their own, which suggest that the critical Shields number tends to a value a little larger than 0.1 for small particle Reynolds numbers, while it tends to be reduced to lower values as the particle Reynolds number increases up to 100. In the present simulations, the particle Reynolds number may be calculated from the relation

$$Re_p = \frac{\gamma a^2}{\nu} = \hat{\tau}_s Re \hat{a}^2 \tag{28}$$

and is found to be 18 for *Re* equal to 3500. Thus, it may be suggested that the present results have an interesting semiquantitative agreement with experimental data from the literature. However, such an agreement should not be overestimated given the two-dimensional character of the simulations.

3.2. Particle Flux vs Shields Number. As expected, when the Reynolds number and the sediment shear stress increase, more particles enter the suspended state and are carried by the fluid. A qualitative picture showing increasing numbers of suspended particles with the Reynolds number may be obtained from Figure 4. The flow snapshots also show color-coded contours of the velocity component in the mean flow direction. An arbitrary chromatic scale is used as shown in the figure. Evidently, the highest velocities appear in the particle-free layer above the sediment, whereas within the sediment near the bottom plate the velocities are zero.

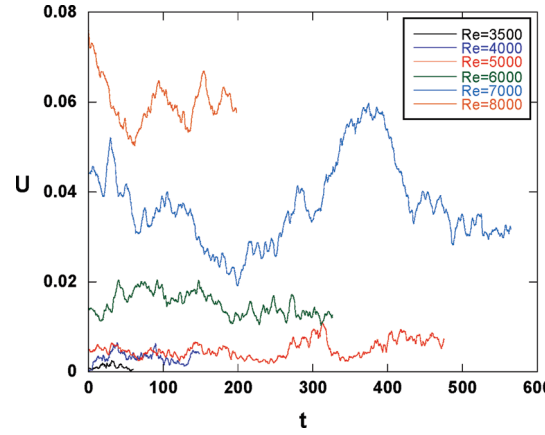

Figure 5. Average particle velocity as a function of (dimensionless) time for the Reynolds numbers indicated.

A more quantitative picture of this behavior may be obtained from Figure 5. Here, the average particle velocity (over the 200 particles) in the main flow direction is plotted as a function of time. Apart from the increased values at increased Reynolds numbers, it is also observed that fluctuations exist in the average particle velocity, and hence in the particle flux, which take place over time scales much longer than the flow time scale.

In order to test the effect of numerical resolution on these results, a simulation with a finer grid was carried out at the highest Reynolds number of 8000. The refined grid had twice as many nodes in each direction and about four times the number of Lagrange multipliers within each particle. The simulation started with the same initial condition interpolated from the results of the basic grid. A comparison of the evolution of the particle average velocity with the basic and the refined grids is shown in Figure 6. Although the two results do not coincide,

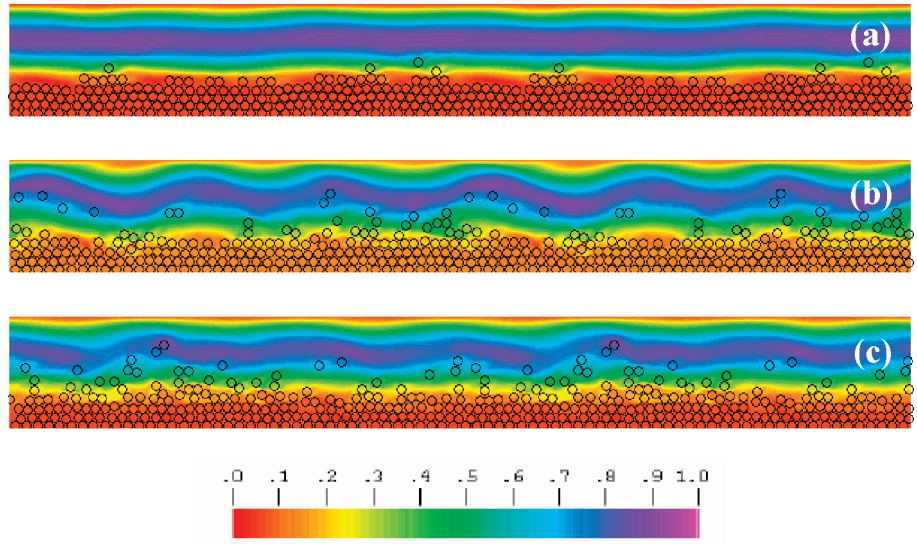

Figure 4. Instantaneous particle positions and color coded contours of the velocity component in the mean flow direction. (a) *Re* = 4000, (b) *Re* = 6000, (c) *Re* = 8000. In the chromatic scale, 1 (purple) corresponds to the maximum value, and 0 (red) corresponds to the minimum.

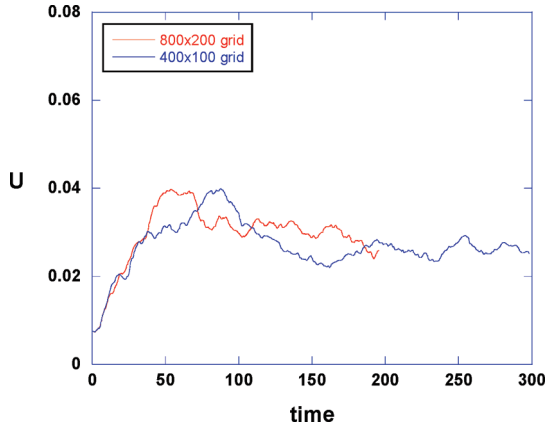

Figure 6. Average particle velocity as a function of time for $Re = 8000$ and two different grids.

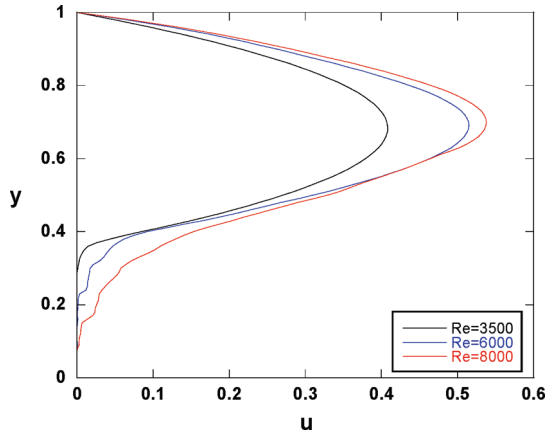

Figure 7. Time-average velocity in the mean flow direction as a function of the distance between the plates.

something that would be highly surprising given the size of the dynamical system of the particles alone, the comparison is favorable in terms of the trend, the mean value and its fluctuations. This lends credence to the accuracy of the results presented and suggests that the fluctuations are not an artifact of poor numerical resolution. Regarding the fluctuations, however, it must be noted here that an additional factor may be possibly responsible, namely the relatively small number of particles. This issue remains open for future investigation, although reasonable statistical behavior has been obtained in other settings (i.e., sedimentation) in the literature and in our lab with simulations employing fewer particles.

In Figure 7, the time-average velocity of the suspension is shown as a function of the distance between the channel plates, for selected Reynolds numbers. The change in the average velocity profile near the lower plate suggests that more particle layers begin to be sheared and enter the suspended state at higher Reynolds numbers.

A practically important piece of information, relevant to problems of sediment transport, is the relation between particle flux and the flow intensity. The latter is reflected in the shear stress on the sediment surface and is usually expressed in terms of the Shields number. Guazzelli et al.[4,5] presents a collection of numerous expressions which have been proposed in the literature to correlate such data. Various power law dependencies exist ranging from linear to cubic. However, the most commonly used expressions[4,7,37] have an exponent close to 1.5 or 2. In Figure 8, the time-average particle flux obtained from the simulations is plotted as a function of Reynolds number, as well

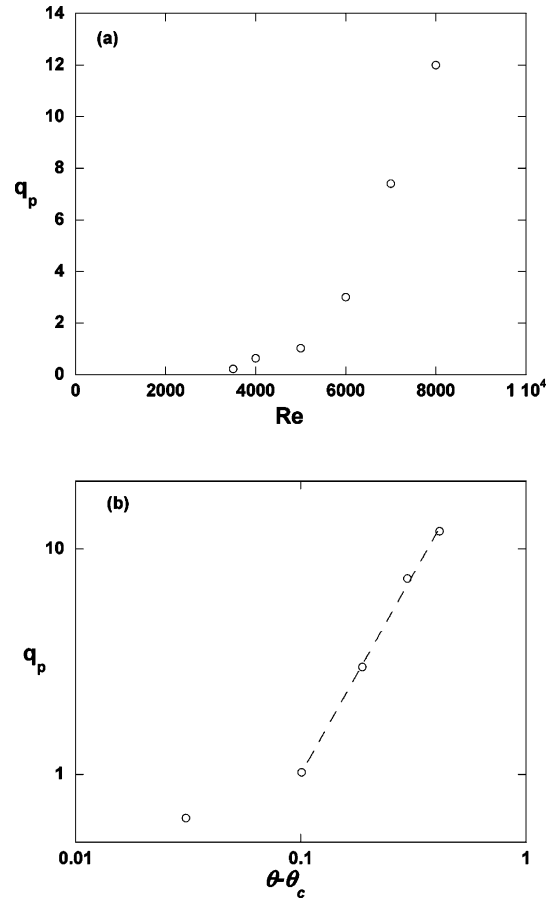

Figure 8. Particle flux as a function (a) of Reynolds number and (b) of the excess Shields number.

as a function of the excess Shields number. As may be interestingly observed from Figure 8b, the data from the present simulations appear to give a similar dependency, with the exception of one point at very small excess Shields number (at $Re = 4000$). The power law exponent obtained is 1.77.

3.3. Flow Instabilities. As has already been mentioned, the particle flux manifests fluctuations on very long time scales. It was also shown in Figure 4 that the velocity contours display a waviness characteristic of an unstable flow. Indeed, in all the simulations waves of velocity and particle concentration appeared to grow while being convected downstream. Similar waves have been found in the simulations of Choi and Joseph,[19] as well as those of Lundgren.[38] In contrast, they were not found by Yan and Koplik,[39] perhaps due to differences in the parameters, but also due to the short length of the periodic channel used in their simulations. This behavior is clearly reminiscent of the instabilities in coflowing adjacent sheared layers with different properties.[40,41] Similar instabilities have also been found to exist is sedimenting suspensions of Brownian particles,[42] where instead of a jump in the properties a gradual transition may exist from sediment to clear fluid.

An interesting feature observed in the present simulations is that as the fluctuations grow to large amplitude their characteristic wavelength tends to change. This behavior may be observed in Figure 9, where snapshots are shown of horizontal velocity contours and particle positions at $Re = 8000$. Within the two adjacent periodic intervals drawn, the number of the dominant waves changes from to 6 to 4, and then from 4 to 2. In order to test whether this behavior was an artifact of the finite length of the periodic flow domain, a simulation was undertaken where this length was doubled. The number of nodes in the

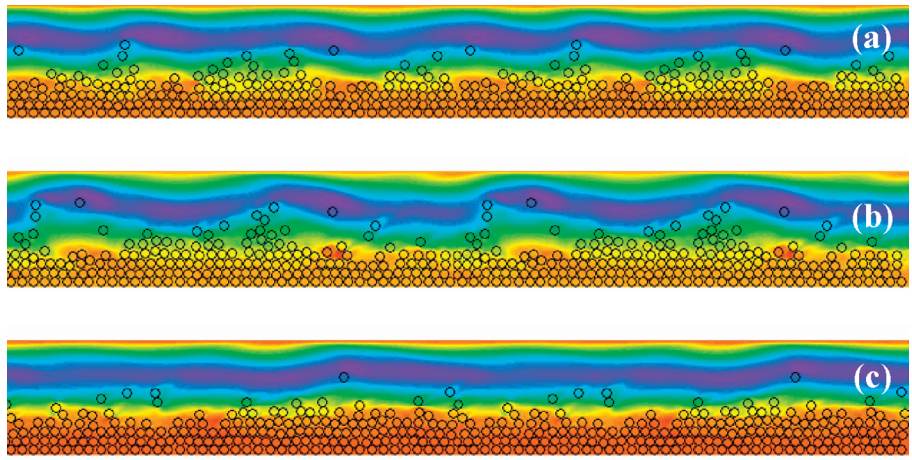

Figure 9. Difference in the fluctuation wavelength at different instants in time, as depicted by the instantaneous particle positions and color coded velocity contours: (a) $t = 120$, (b) $t = 255$, (c) $t = 390$.

Table 2. Parameters of the mDEM

c_1	250 (N/m)
c_2	1.2×10^{-3} (N s/m)
c_3	12.5 (N/m)
c_4	0.003 (N s/m)
c_5	6.2×10^{-7} (N m)
c_6	9.3×10^{-11} (N m s)
μ	0.2
μ_t	10^{-6} m

flow direction and the number of particles were doubled accordingly. The results in this extended flow domain did not show any further coarsening of the waveforms. It is verified in this way that the qualitative behavior described above is not an artifact of the periodic geometry and that the basic periodic length chosen is sufficient to capture the essential dynamics of the waveforms generated.

This wave coarsening behavior is reminiscent of the coarsening of sand ripples and dunes formed during the steady flow of air and water or during the oscillating flow created by water waves. The formation of ripples and other bed forms has attracted the interest of many researchers for many years. The subject has also seen a revived interest in recent years and many theoretical and experimental studies have appeared, which examine the shape instability of beds exposed to turbulent flow or to the flow of viscous fluids.[4,5,9−12,43−46] The instability is invariably attributed to a phase lag between the sinusoidally perturbed shape of an erodible bed and the shear stress exerted by the clear fluid flowing above it. However, it has been suggested that the influence of the flowing particles above the bed on the fluid flow is an important issue not adequately elucidated.[5,46] The present results clearly suggest that such an instability, related to the dynamics of the flowing layer of particles above the sediment, indeed exists. The link between this instability and the morphodynamics of ripples and dunes is a question that remains to be addressed.

3.4. Effects of Particle Micromechanical Interactions. In this final subsection, the issue of particle collisions is touched upon. For this purpose, the mDEM, which was presented in the previous section, replaced the simpler central force model in the simulation code. If particles of radius 1 mm are assumed, the model parameters used are shown in Table 2. These were selected on the basis of the previously employed central forces and additional numerical experiments with particles bouncing on a flat surface in vacuum.

Four series of simulations at $Re = 5000$, 6000, 7000, and 8000 were performed. The final states of the previous series,

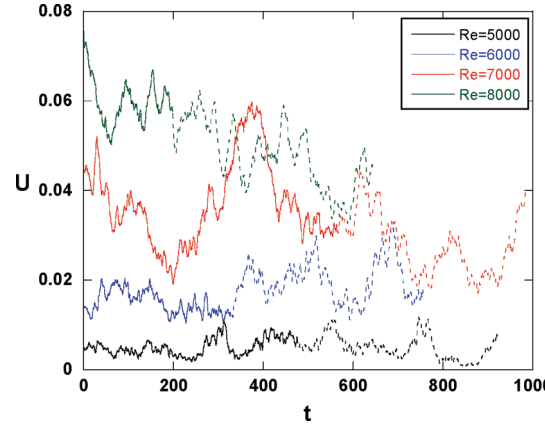

Figure 10. Average particle velocity as a function of time for the Reynolds numbers indicated. The switch from the simple central force model to the mDEM is marked by the points in time where the lines become dashed.

obtained with the simpler force model, were used as initial conditions in an effort to see possible changes in the behavior of the system. No dramatic changes in the collective particle behavior or the characteristics of the fluid motion were detected. Figure 10 shows the behavior of the particle average velocity as a function of time. Results with the simpler central force model are also shown by the continuous lines for comparison. The switch to the mDEM model is marked by the points in time where the lines become dashed. Probably at the higher Reynolds numbers, there is a small gradual decline in the mean particle velocity due to the energy dissipation introduced by the model during the collisions. However, given that the overall behavior is marked by significant fluctuations, it may be argued that no dramatic change is detected. Of course, in order to provide more conclusive statements, a much more thorough study is needed and the model parameters also need to be systematically and judiciously modified. However, it may be added here that this first conclusion is not at variance with the numerical observations of Wee et al.[31] who modeled pneumatic transport by a (volume averaged) CFD model for fluid flow coupled with a DEM for particle collisions. It is also not at variance with the assessment of Heald et al.,[37] who employed a DEM for particle collisions and a very simplified form of particle−flow interactions.

4. Summary and Concluding Remarks

A DNS methodology for fluid flow and particle motion was employed to study the incipient sediment motion and the first stages of hydraulic transport. On the basis of the simulations, a critical Shields number was identified and the dependence of particle flux on the flow intensity was found. Both results showed an encouragingly favorable comparison with existing literature data.

The fluid flow and the moving sediment were found to be unstable and to display characteristic waves, which coarsened during the course of the simulations in a way similar to the coarsening of ripples in sand beds exposed to water or air flows. The present results clearly suggest that a type of hydrodynamic instability related to the sheared layer of moving particles above the sediment is operative. It appears plausible to suggest that this instability may also be related to the pattern formation on the sediment surface and, hence, on the friction experienced by the fluid. The latter issues are critical in the prediction of the behavior of conveying systems.

The methodology for fluid flow simulation was coupled to a DEM for particle collisions in order to have an improved degree of realism in the particle interactions during their collisions. A combination of a DEM model with a DNS approach for the fluid flow has appeared in the literature only once before,[32] at the time of the writing of the present paper. However, no dramatic differences were found with the DEM model over the simpler model of central elastic forces. This observation, which is not at variance with previous results in the literature, may not be surprising since the resuspended particle layer is not necessarily a very dense particulate system. Nevertheless, it appears reasonable to suggest that the DNS/DEM combination may prove valuable in describing the system behavior in other regions of the parameter space or in other problems of particle-laden flows. It is, thus, suggested that numerical approaches along the lines of the present work may be useful in the fundamental study of complex particle laden flows and also that further work may assist in the direction of improved design of such systems.

Acknowledgment

This paper is dedicated to Professors A. J. Karabelas and S. G. Nychas on the occasion of their retirement. They have been teachers to all of us and to thousands more chemical engineers in Greece, and, in addition, the senior author (SGY) collaborated with Professor A. J. Karabelas for many years.

Literature Cited

(1) Rabinovich, E.; Kalman, H. Pickup, critical and wind threshold velocities of particles. *Powder Tech.* **2007**, *176*, 9.

(2) Rabinovich, E.; Kalman, H. Incipient motion of individual particles in horizontal particle-fluid systems: A. Experimental analysis. *Powder Tech.* **2009**, *192*, 318.

(3) Kuru, W. C.; Leighton, D. T.; McCready, M. J. Formation of waves on a horizontal erodible bed of particles. *Int. J. Multiphase Flow* **1995**, *21*, 1123.

(4) Ouriemi, M.; Aussillous, P.; Guazzelli, E. Sediment dynamics. Part 1. Bed-load transport by laminar shearing flows. *J. Fluid Mech.* **2009**, *636*, 295.

(5) Ouriemi, M.; Aussillous, P.; Guazzelli, E. Sediment dynamics. Part 2. Dune formation in pipe flow. *J. Fluid Mech.* **2009**, *636*, 321.

(6) Engelund, F.; Fredsoe, J. Sediment ripples and dunes. *Annu. Rev. Fluid Mech* **1982**, *14*, 39.

(7) Lobkovsky, A. E.; Orpe, V.; Molloy, R.; Kudrolli, A.; Rothman, D. H. Erosion of a granular bed driven by laminar fluid flow. *J. Fluid Mech.* **2008**, *605*, 47.

(8) Mazumder, R. J. Sediment transport, aqueous bedform stability and morphodynamics under unidirectional current: a brief overview. *J. Afr. Earth Sci.* **2003**, *36*, 1.

(9) Charru, F.; Mouilleron, H.; Eiff, O. Erosion and deposition of particles on a bed sheared by a viscous flow. *J. Fluid Mech.* **2004**, *519*, 55.

(10) Charru, F.; Hinch, E. J. Ripple formation on a particle bed sheared by a viscous liquid. Part 1. Steady flow. *J. Fluid Mech.* **2006**, *550*, 111.

(11) Charru, F.; Hinch, E. J. Ripple formation on a particle bed sheared by a viscous liquid. Part 2. Oscillating flow. *J. Fluid Mech.* **2006**, *550*, 123.

(12) Colombini, M. Revisiting the linear theory of sand dune formation. *J. Fluid Mech.* **2004**, *502*, 1.

(13) Prosperetti, A.; Tryggvason, G., Eds.; *Computational Methods for Multiphase flow*; Cambridge University Press: New York, 2007.

(14) Tsuji, Y. Multi-scale modeling of dense phase gas-particle flow. *Chem. Eng. Sci.* **2007**, *62*, 3410.

(15) van der Hoef, M. A.; Ye, M.; van Sint Annaland, M.; Andrews, A. T.; Sundaresan, S.; Kuipers, J. A. M. Multiscale modeling of gas-fluidised beds. *Adv. Chem. Eng.* **2006**, *31*, 65.

(16) Snider, D. M.; O'Rourke, P. J.; Andrews, M. J. Sediment flow in inclined vessels calculated using a multiphase particle-in-cell model for dense particle flows. *Int. J. Multiphase Flow* **1998**, *24*, 1359.

(17) Owoyemi, O.; Mazzei, L.; Lettieri, P. CFD Modeling of Binary-Fluidized Suspensions and Investigation of Role of Particle-Particle Drag on Mixing and Segregation. *AIChE J.* **2007**, *53*, 1924.

(18) Johnson, A. A.; Tezduyar, T. E. 3D simulation of fluid-particle interactions with the number of particles reaching 100. *Comput. Methods Appl. Mech. Eng.* **1997**, *145*, 301.

(19) Choi, H. G.; Joseph, D. D. Fluidization by lift of 300 circular particles in plane Poiseuille flow by direct numerical simulation. *J. Fluid Mech.* **2001**, *438*, 101.

(20) Glowinski, R.; Pan, T.-W.; Hesla, T. I.; Joseph, D. D. A distributed Lagrange multiplier/fictitious domain method for particulate flows. *Int. J. Multiphase Flow* **1999**, *25*, 755.

(21) Pozrikidis, C. *Boundary Integral and Singularity Methods for Linearized Viscous Flow*; Oxford University Press: New York, 1997.

(22) Brady, J. F.; Bossis, G. Stokesian dynamics. *Annu. Rev. Fluid Mech.* **1988**, *20*, 111.

(23) Yin, X.; Koch, D. L. Hindered settling velocity and microstructure in suspensions of solid spheres with moderate Reynolds numbers. *Phys. Fluids* **2007**; 093302.

(24) Hill, R. J.; Koch, D. L.; Ladd, A. J. C. The first effects of fluid inertia on flows in ordered and random arrays of spheres. *J. Fluid Mech.* **2001**, *448*, 213.

(25) Peskin, C. S. The immersed boundary method. *Acta Num.* **2002**, *11*, 479.

(26) Glowinski, R.; Pan, T. W.; Hesla, T. I.; Joseph, D. D.; Periaux, J. A fictitious domain approach to the direct numerical simulation of incompressible viscous flow past moving rigid bodies: application to particulate flow. *J. Comput. Phys.* **2001**, *169*, 363.

(27) Iwashita, K.; Oda, M. Rolling resistance at contacts in simulation of shear band development by DEM. *J Eng. Mech.* **1998**, *124*, 285.

(28) Zhu, H. P.; Zhou, Z. Y.; Yang, R. Y.; Yu, A. B. Discrete particle simulation of particulate systems: Theoretical developments. *Chem. Eng. Sci.* **2007**, *62*, 3378.

(29) Kafui, K. D.; Thornton, C.; Adams, J. Discrete particle-continuum fluid modeling of gas-solid fluidised beds. *Chem. Eng. Sci.* **2002**, *57*, 2395.

(30) Guo, Y.; Kafui, K. D.; Wu, C.-Y.; Thornton, C.; Seville, J. P. K. A coupled DEM/CFD analysis of the effect of air on powder flow during die filling. *AIChE J.* **2009**, *55*, 49.

(31) Wee, E.; Lim, C.; Wang, C.-H.; Yu, A.-B. Discrete element simulation for pneumatic conveying of granular material. *AIChE J.* **2006**, *52*, 496.

(32) Wachs, A. A DEM-DLM/FD method for direct numerical simulation of particulate flows: Sedimentation of polygonal isometric particles in a Newtonian fluid with collisions. *Comput. Fluids* **2009**, *38*, 1608.

(33) Pan, T. W.; Joseph, D. D.; Glowinski, R. Modeling Rayleigh-Taylor instability of a sedimenting suspension of several thousand circular particles in a direct numerical simulation. *J. Fluid Mech.* **2001**, *434*, 23.

(34) Pan, T.-W.; Glowinski, R. Direct simulation of the motion of neutrally buoyant circular cylinders in plane Poiseuille flow. *J. Comput.Phys.* **2002**, *181*, 260.

(35) Pan, T.-W.; Joseph, D. D.; Bai, R.; Glowinski, R.; Sarin, V. Fluidization of 1204 spheres: simulation and experiment. *J. Fluid Mech.* **2002**, *451*, 169.

(36) Loiseleux, T.; Gondret, P.; Rabaud, M.; Doppler, D. Onset of erosion and avalanche for an inclined granular bed sheared by a continuous laminar flow. *Phys. Fluids* **2005**, *17*, 103304.

(37) Heald, J.; McEwan, I.; Tait, S. Sediment transport over a flat bed in a unidirectional flow: simulations and validation. *Phil. Trans. R. Soc. Lond. A* **2004**, *362*, 1973.

(38) Apte, S. V.; Mahesh, K.; Lundgren, T. Accounting for finite-size effects in simulations of disperse particle-laden flows. *Int. J. Multiphase Flow* **2008**, *34*, 260.

(39) Yan, Y.; Koplik, J. Transport and sedimentation of suspended particles in inertial pressure-driven flow. *Phys. Fluids* **2009**; 013301.

(40) Yih, C. S. Instability due to viscosity stratification. *J. Fluid Mech.* **1967**, *27*, 337.

(41) Yiantsios, S. G.; Higgins, B. G. Linear stability of plane Poiseuille flow of two superposed fluids. *Phys. Fluids* **1988**, *31*, 3225.

(42) Yiantsios, S. G. Plane Poiseuille flow of a sedimenting suspension of Brownian hard-sphere particles: Hydrodynamic stability and direct numerical simulations. *Phys. Fluids* **2006**, *18*, 054103.

(43) Colombini, M.; Stocchino, A. Finite-amplitude river dunes. *J. Fluid Mech.* **2008**, *611*, 283.

(44) Charru, F. Selection of the ripple length on a granular bed sheared by a liquid flow. *Phys. Fluids* **2006**, *18*, 121508.

(45) Mouilleron, H.; Charru, F.; Eiff, O. Inside the moving layer of a sheared granular bed. *J. Fluid Mech.* **2009**, *628*, 229.

(46) Larrieu, E.; Hinch, E. J.; Charru, F. Lagrangian drift near a wavy boundary in a viscous oscillating flow. *J. Fluid Mech.* **2009**, *630*, 391.

Received for review January 13, 2010
Revised manuscript received May 8, 2010
Accepted May 19, 2010

IE1000828